UNIVERSITÀ DEGLI STUDI DI PADOVA

Department of Physics and Astronomy
"Galileo Galilei"

Bachelor Degree Course in
Astronomy

Bachelor Degree Thesis

Constraints on the Neutron Star equation of state from multiwavelength observations of the event GW170817

Supervisor:

Prof. Roberto Turolla

Candidate:

Alberto Salvarese

Serial number: 1142643

Academic Year 2018/2019

Abstract

In this bachelor degree thesis I describe one of the possible process of formation of a neutron star (NS) and its internal structure. Then I briefly derive the TOV equation, explaining the meaning of the gravitational mass and the role of the pressure in a general relativistic context. Furthermore I derive the equation of state of an ideal Fermi-gas of electrons and nucleons starting from the calculation of the number of available quantum states. Finally, I describe the first model of neutron stars, briefly highlighting the two extreme limits for the equations of state.
In the second chapter I describe the event GW170817, trying to defining all phenomenon like kilonova or GRB. Then, I summarize the studies on the constraints on the merger remnant, which resulted to be a HMNS or a short-lived SMNS, on the maximum mass ($M_{TOV} \lesssim 2.17 M_{\odot}$) of a neutron star and on the their radii ($R_{max} \geq 9.60^{+0.14}_{-0.03}$km) obtained by the observations of gravitational and electromagnetic waves. Finally I underline the constraints on the high density equations of state set by the results inferred by GW170817.

Contents

Introduction

Neutron Stars represent the densest objects known in the universe nowadays. Despite a lot of years of observations and studies, the properties of the matter under such conditions are still unknown. The problem of the so called *Equation of State* of this material is one of the most important issues of the modern astrophysics. The gravitational wave event GW170817 occured on August 17, 2017 and involved the merging of two neutron stars in a binary system shed light on the possible properties of these objects and on their internal composition and behaviour. In this bachelor degree thesis I briefly describe the compact objects known as neutron stars and the event GW170817 with its implications.
The thesis starts with the description of Neutron Stars formation process as the remnant of a massive star supernova explosion and it continues with a brief derivation of the equation that describes the condition of Hydrostatic Equilibrium (HE) in a General Relativistic context. I then describe a so called Fermi-gas, i.e., a gas composed by fermions, which in the case discussed here are electrons and nucleons. I derive the expression for the number density, the energy density and the pressure and I underline the conditions of chemical equilibrium and the asymptotic proton density in a ultra-relativistic regime ($n_p \to \frac{1}{8} n_n$) which is why neutron stars are though to be composed mostly of neutrons. I described also the first neutron star model and the difference between stiff and soft equations of state.
Later I report the observations of the event GW170817 and introduce a brief description of two of its electromagnetic counterparts: Kilonova and Gamma-Ray Burst. The thesis proceeds summarizing the studies about the data inferred and their implications. From these I summarize different studies in order to constrain the values of the maximum mass and radius of a non rotating neutron star, through three different methods, supported both by analytical or semi-analytical and by numerical approaches. Finally I present the constraints on the equations of state, obtained by comparisons between the values predicted by these equations and the ones obtained through the previous discussions.
In the end, the restrictions of these procedures are reported. These are mostly given by the limits that can affect the experimental equipment and by the impossibility to completely justify some hypothesis or assumptions, due to the fact that some events, like kilonova, are still not sufficiently known. However the consistency between the different methods followed and all assumptions used are underlined and proved as possible. I conclude highlighting the importance of future events which can include GW and EM emission to refine the constraints on all NS properties and, especially, on the high density matter equation of state.

Chapter 1

Neutron Stars

A Neutron Star is a small and very compact object ($r_{NS} \sim 9 - 11.5$km, $\rho_{NS} \geq 10^{14}$ gcm^{-3}, in the centre), formed at the end of the evolution of a massive star and composed by degenerate material. Neutron Star are usually observed as pulsating radio sources called Pulsars. A Pulsar is a star with an intense magnetic field ($\sim 10^{12}$ G) that is observed emitting radio wave beams from its magnetic poles.
Neutron Stars were introduced by Landau [1] and by Baade and Zwicky [2] as possible remnants of Supernova explosions. Several pulsars were discovered in the following years [3, 4] and the confirmation of the correlation between pulsars and supernovae came with the discover of a pulsar in the Vela supernova and in the Crab Nebula remnants [5, 6] .

1.1 The process of formation of Neutron Stars

A star of at least $M \simeq 1.1 M_{\odot}$ ignites carbon in its core ($T \geq 5 \cdot 10^8 K$). After the burning of carbon, the following steps of stellar evolution are a rapid series of ignitions and contractions which increase the central temperature of the star. These processes end when a massive star ($M \geq 11 M_{\odot}$) forms a core of elements of the iron group (^{56}Fe). When the star produces ^{56}Fe, due to several processes that result in neutrinos emission during the carbon ignition, its core appears to be in a state of electron degeneracy [7], in which electrons are always relativistic because of the high temperature and density ($\geq 10^9$ gcm^{-3}). In this case contraction cannot be stopped and it continues on a very rapid thermal timescale. Furthermore there are two processes that accelerate the already fast collapse: Electron Capture and Photo-Disintegration.
The first process leads to an increase of neutrons and neutrinos through the reaction

$$e^- + p \rightarrow n + \nu_e.$$

The neutrinos escape very quickly from the star, due to their large mean free path, taking away energy from the core. Furthermore the endothermic photo-disintegration process

$$\gamma + \ ^{56}Fe \rightarrow 13 \ ^4He + 4n$$

subtracts other energy from the core. These two processes, subtrating internal energy, reduce the ability of the star to contrast its own collapse. During the following rapid collapse, temperature and density rise up but not enough to stop it, until nuclear densities are reached ($\sim 10^{14}$ gcm^{-3}).

Further inverse β-decay and photo-disintegration processes can occur, increasing the degree of neutronization of the core. Before the core reaches the nuclear densities, when $\rho/\mu_e \sim 4 \cdot 10^9$ gcm^{-3}, the mean free path of neutrinos becomes similar to the typical sizes of the collapsing core so that they cannot escape freely from it. Moreover, when $\rho_{core} \geq 3 \cdot 10^{11}$ gcm^{-3}, the diffusion velocity of neutrinos becomes lower than the velocity of the infalling material. Therefore the core becomes opaque to neutrinos and this congestion makes them degenerate since they are fermions and all energy states become occupied.
In the conditions reached at the end of the collapse, another compression leads to a violent shock wave. This shock wave, helped by the energy of neutrinos trapped in the core, cause an explosion that ejects most of the material outside the core in the surrounding space.
This explosion is the so called **Supernova** (**SN**) and the remnant of this phenomenon, if the mass of the star is small enough ($M \leq 20 - 30 M_\odot$), will be a nebula which surrounds the remains of the stellar core: a **Neutron Star** (**NS**). If instead the stellar mass is bigger than $\sim 30 M_\odot$, then the kinetic energy generated by collapse decreases and the binding energy increases. If the generated explosion is weak enough, then the material ejected may fall back in the just-formed neutron star exceeding the maximum possible mass and causing its collapse giving birth to a **Black Hole**(**BH**). However, since the final stages of stellar evolution are still not completely understood, the divide between stellar masses that form NS and those that form BH is uncertain [8, 9].

1.2 The structure of Neutron Stars

The structure of a NS can be schematically divided in three different layers, that proceeding inwards are: the *outer crust*, the *inner crust* and the *core*. The composition of the outermost layers of a NS is determined by observations (it is mostly composed by iron-group elements), while the innermost regions composition is uncertain because of the lack of obtainable data. [8–10].

- ***Outer crust***: it is roughly ~ 0.3 km thick and has a density between $\sim 10^6$ gcm^{-3} and $\sim 4.3 \cdot 10^{11}$gcm^{-3}. It is composed by a lattice of heavy nuclei surrounded by an electron gas.In this part of the star the pressure is provided by the electron degeneracy pressure. Moving towards the internal boundary, the density and pressure increase so that the inverse β-decay become more efficient making the nuclei more neutron rich, until neutrons become unbound and start to evaporate from the nuclei *neutron drip point*. This marks the beginning of the inner crust.

- ***Inner crust***: This layer is ~ 0.5 km thick and it is denser than the outer crust. Its density is in the range $[4.3 \cdot 10^{11}, 2 \cdot 10^{14}]$ gcm^{-3}. Here the main contribution to the pressure is provided by the neutron gas.
  In this layer, matter is composed by two different phases: the first one is a lattice of neutron-rich nuclei which is immersed in the other phase, which consists of a neutron gas ("*neutron ocean*" [10]).
  When the density of the material reaches values $\rho_0 \approx 2 \cdot 10^{14}$ gcm^{-3}, the two phases are not separate anymore and together form an unique fluid of protons, electrons and neutrons, whit no net global due to the presence of the electron gas.

- ***Core***: Inside the inner crust there is a homogeneous fluid of p, n, e^- in β-equilibrium. Several other processes can however occur at these extreme densities ($\geq 10^{14}$ gcm^{-3}).

For example the following reaction can occur

$$n \to p + \mu^- + \bar{\nu_\mu},$$

in which a neutron decays into a proton, a muon and a μ-neutrino that escapes from the star. It could be shown that in the core the main contribution of the pressure is given by neutrons. Even the total energy is provided mostly by neutrons, since they have a larger mass than electrons.
Due to the extremely high densities, neutrons have to be treated as ultrarelativistic particles.

1.3 The Hydrostatic Equilibrium

Due to the nature of the class of compact objects, to which Neutron Stats belong, the relation for the Hydrostatic Equilibrium (HE) founded from the second law of dynamics ($\vec{F} = m\vec{a}$),

$$\frac{\partial P}{\partial r} = -\frac{\rho(r) G m(r)}{r^2}, \tag{1.1}$$

is no longer valid. NSs and other compact objects imply gravitational fields that need to be described by the theory of General Relativity (GR).
Very strong gravitational fields are described by Einstein's field equations:

$$R_{ik} - \frac{1}{2} g_{ik} R = \frac{\kappa}{c^2} T_{ik}, \qquad \kappa = \frac{8\pi G}{c^2}, \tag{1.2}$$

where R_{ik} is the Ricci tensor, g_{ik} is the metric tensor and $R = g_{ik}R^{ik}$ is the Riemann curvature. T_{ik} represents the energy-momentum tensor, whose non-zero components are, in the case of a perfect fluid,

$$T_{00} = \rho c^2, \; T_{11} = T_{22} = T_{33} = P,$$

where ρ represents the *mass-energy density* and P is the isotropic pressure.
For the case of a static and spherically symmetric space-time, the line element ds, that represents the space-time distance between two neighbouring events, can be represented in spherical coordinates (r, θ, ϕ) as the following general form

$$ds^2 = -A(t,r)c^2dt^2 + B(t,r)dr^2 + 2C(t,r)cdtdr + D(t,r)d\Omega^2$$

where $d\Omega^2 = d\theta^2 + \sin^2\theta d\phi^2$. Now, by choosing a new radial coordinate $r' = D^{1/2}(t,r)$ and substituting it in the above expression, one has:

$$ds^2 = -E(t,r)c^2dt^2 + F(t,r)dr^2 + 2G(t,r)cdtdr + r^2d\Omega^2$$

where E, F and G are functions related to A, B and C given by the substitution of r. It is possible to eliminate the coefficient of $dtdr$ using another susbtitution, for example choosing t' such that $dt' = E(t,r)dt - G(t,r)dr$. In general this differential form is not exact, however it can be possible demonstrate that an integrating-factor $K(t,r)$, such that the differential form $K(t,r)dt'$ is exact, always exists. Substituting:

$$ds^2 = -e^\nu c^2dt^2 + e^\lambda dr^2 + r^2(d\theta^2 + \sin^2\theta d\phi^2),$$

where $e^{\nu},\ e^{\lambda}$ are integral-factors and $\nu = \nu(r)$ and $\lambda = \lambda(r)$ are fantions of r.

With this expressions for T_{ik} and ds^2, the equations (1.2) can be reduced to the following set of ordinary differential equations:

$$\frac{\kappa P}{c^2} = e^{-\lambda}\left(\frac{\nu'}{r} + \frac{1}{r^2}\right) - \frac{1}{r^2} \tag{1.3}$$

$$\frac{\kappa P}{c^2} = \frac{1}{2}e^{-\lambda}\left(\nu'' + \frac{\nu'^2}{2} + \frac{\nu' - \lambda'}{r} - \frac{\nu'\lambda'}{2}\right) \tag{1.4}$$

$$\kappa\rho = e^{-\lambda}\left(\frac{\lambda'}{r} - \frac{1}{r^2}\right) + \frac{1}{r^2}. \tag{1.5}$$

Multiplicating for $4\pi r^2$ eq. (1.5) and integrating over r, it results:

$$\begin{aligned}
\int_0^r \kappa 4\pi r^2\rho\ dr &= \int_0^r 4\pi r^2\left(e^{-\lambda}\left(\lambda' - \frac{1}{r^2}\right) + \frac{1}{r^2}\right)\ dr \\
&= 4\pi\int_0^r e^{-\lambda}r\lambda' - e^{-\lambda} + 1\ dr \\
&= 4\pi\left(r + \int_0^r e^{-\lambda}r\lambda' - e^{-\lambda}\ dr\right) \\
&= 4\pi\left(r - e^{\lambda}r + \int_0^r e^{-\lambda}\ dr - \int_0^r e^{-\lambda} + 1\ dr\right) \\
&= 4\pi r(1 - e^{-\lambda})
\end{aligned}$$

where $\lambda' = \frac{d\lambda}{dr}$.
By defining $dm^g = 4\pi r^2\rho\ dr$, it follows

$$\kappa M^g = 4\pi r(1 - e^{-\lambda}). \tag{1.6}$$

The quantity m^g is so that at radius $r = R_{tot}$, it becomes M^g, the gravitational mass of the whole star. The integral form of M^g could be considered at first as the total baryonic mass of the star, but actually it doesn't represent only this value. Indeed it contains not only the rest mass of the star, but also its total energy, including the gravitational contributes. One can see it by considering that $\rho = \rho_0 + U/c^2$ indicates the mass-energy density, which contains the total energy density U/c^2 and the rest-mass density ρ_0; furthermore the changed metric would give the spherical volume element as $e^{\lambda/2}4\pi r^2 dr$ (eq. 1.7) and not the typical form $4\pi r^2 dr$.
Indeed, by considering the proper volume of the star V_p, the other volumes observed are related to the proper one as $dV = \gamma_{GR}dV_p$ where $\gamma_{GR} = \sqrt{ds^2}|_{dt=d\theta=d\phi=0} = e^{\lambda/2}$. So, by defining M_0 as the rest mass of the star, one obtains:

$$dm_0 = \rho(r)dV_p = \rho(r)e^{\lambda/2}dV \tag{1.7}$$

where from eq. (1.6) $e^{\lambda/2} = \left(1 - \frac{2M^g G}{rc^2}\right)^{-1/2}$. By using the approximation $\frac{2M^g G}{r} << c^2$, then $e^{\lambda/2} \approx 1 + \frac{M^g G}{rc^2}$. Thus:

$$\begin{aligned} M_0 &= \int_0^{R_{tot}} \rho(r) \left(1 + \frac{M^g G}{rc^2}\right) 4\pi r^2 dr \\ &= \int_0^{R_{tot}} \rho(r) 4\pi r^2 dr + \frac{1}{c^2} \int_0^{R_{tot}} \frac{M^g G}{r} \rho(r) 4\pi r^2 dr \\ &= M^g + \frac{1}{c^2} \int_0^{M^g} \frac{M^g G}{r} dm^g \\ &= M^g - \frac{U^g}{c^2} \\ M^g &= M_0 + \frac{1}{c^2} U^g \end{aligned} \tag{1.8}$$

where U^g represents the gravitational energy.
Thus, now it is possible to see that the so called *Gravitational Mass* includes all gravitational binding energy contributions.
Now, by differentiating eq. (1.3) on r and by eliminating the values $\lambda, \lambda', \nu', \nu''$ through (1.4),(1.5) and (1.6), one obtains the **Tolman-Oppenheimer-Volkoff equation (TOV)**, that describes the condition of HE of a spherical symmetric star in a GR context (as in the case of a non-rotating NS):

$$\frac{dP}{dr} = -\frac{Gm}{r^2} \rho \left(1 + \frac{P}{\rho c^2}\right) \left(1 + \frac{4\pi r^3 P}{mc^2}\right) \left(1 - \frac{2Gm}{rc^2}\right)^{-1}. \tag{1.9}$$

In the TOV equation pressure and energy density (ρ) appear to set the gradient of pressure. As gravity compresses the material of the star, this replies with an enhancement of the pressure, but since P appears even on the right side of the TOV, this increase raises up the grasp of gravity on the material. Thus gravity increases because of the raising of P, which causes a further increase of gravity and so on. From a critical value of the mass onwards there is no escape from gravitational collapse to a BH [11].
The maximum mass value of a relativistic star, usually called M_{TOV} (if the star is static), depends on the EoS of the star.

1.4 The Fermi Model

The first NS model was made assuming that these stars were composed by an Ideal Fermi-gas. Neutrons, protons and electrons are fermions, thus they obey to the Pauli Exclusion Principle, which establishes that no more than one fermion can occupy a quantum state. The EoS for ad ideal (no interactions between fermions are considered) and fully degenerate (all quantum states of a given energy are occupied) Fermi-Gas can be obtained as follows. In three dimensions, the *number of quantum states* in a volume V with momentum $p = \mid \vec{p} \mid$ between p and $p + dp$ is

$$g(p)dp = g_s \frac{V}{h^3} 4\pi p^2 dp = g_s \frac{V}{(2\pi\hbar)^3} 4\pi p^2 dp,$$

where g_s is the number of intrinsic quantum states of a given particle ($g_s = 2$ for fermions). In general, for non complete degeneracy, the distribution of the available quantum states for fermions is $f_f(p) = \frac{1}{e^{p^2/2m_f kT - \psi} + 1}$ which is always ≤ 1 ($f_f = 1$ when degeneracy is complete). To obtain the number density of fermions $n_f(p)$ one has to multiply $g(p)$ with the distribution written above and integrate over the interval of momenta. In the case of complete degeneracy, from the relations $n = \int_p^{p+dp} n_f(p)dp$, $\epsilon = \int_p^{p+dp} \varepsilon_f(p) n_f(p)dp$ and $P = \int_p^{p+dp} p v_p n(p)dp$ and considering $\varepsilon(p) = \sqrt{p^2c^2 + m^2c^4}$, each fermion (neutrons, protons and electrons) with momentum between 0 and p_f (Fermi momentum) has number density, energy density and pressure given by

$$n(p) = \frac{g_s}{2\pi^2\hbar^3} \int_0^p p^2 dp,$$

$$\epsilon(p) = \frac{g_s}{2\pi^2\hbar^3} \int_0^p \sqrt{p^2c^2 + m^2c^4} p^2 dp, \tag{1.10}$$

$$P(p) = \frac{1}{3} \frac{g_s}{2\pi^2\hbar^3} \int_0^p \frac{p^2c^2}{\sqrt{p^2c^2 + m^2c^4}} p^2 dp.$$

To obtain the equation (1.8) for the pressure another step is necessary; from the general integral relation written above, in the ultrarelativistic limit one can consider $p = \frac{mv}{\sqrt{1 - \frac{v^2}{c^2}}}$, and from the expression of the energy $\varepsilon = \frac{mc^2}{\sqrt{1 - \frac{v^2}{c^2}}}$, it follows that $v = \frac{c^2 p}{\varepsilon}$.
Thus, by solving the integrals (1.8)(an example is given in apendix A) one can obtain:

$$n(p) = \frac{p^3}{3\pi^2\hbar^3},$$

$$\varepsilon(p) = \frac{1}{4\pi^2\hbar^3} \left[\frac{\mu p}{c^2} (\mu^2 - \frac{1}{2} m^2c^4) - \frac{1}{2} m^4c^5 \ln\left(\frac{pc + \mu}{mc^2} \right) \right], \tag{1.11}$$

$$P(p) = \frac{1}{12\pi^2\hbar^3} \left[\frac{\mu p}{c^2} \left(\mu^2 - \frac{5}{2} m^2c^4 \right) + \frac{3}{2} m^4c^5 \ln\left(\frac{pc + \mu}{mc^2} \right) \right],$$

with $\mu = (m^2c^4 + p^2c^2)^{1/2}$ ($p = p_f$) that represents the chemical potential or the Fermi Energy. To minimize the energy of fermions at given baryon density indicated as the density of nucleons ($m_{nuc} \gg m_e$) $n(p) = n_p(p) + n_n(p)$ (thus, to obtain an equilibrium state of the gas), and requiring the condition of charge neutrality (stars are not electrically charged) $n_p(p) = n_e(p)$, one can use the Lagrangian multipliers.
The condition given by this method for the minimum of the energy is (A.2)

$$\mu_n = \mu_p + \mu_e. \tag{1.12}$$

This condition called *Chemical Equilibrium* shows that the particles levels are so filled that no energy can be extracted from gas via beta decay of a neutron or an electron capture by a proton (β-equilibrium).
From the first (1.9) equation it follows that the Fermi momenta of nucleons are related to the baryon density (thanks to the condition for the baryon density):

$$\frac{1}{3\pi^2\hbar^3}(p_p^3 + p_n^3) = n(p). \tag{1.13}$$

The condition that expresses the charge neutrality, using the equation for the number density, can be written as $p_p = p_e$. These last two equations can be combined with the eq. (1.10) to calculate p_p,p_n and p_e such that energy can be minimized.
Supposing $p_p = 0$:

$$\begin{aligned}(m_n^2c^4 + p_n^2c^2)^{1/2} &= (m_p^2c^4 + p_p^2c^2)^{1/2} + (m_e^2c^4 + p_e^2c^2)^{1/2} \\ &= m_pc^2 + m_ec^2\end{aligned}$$

$$p_n^2c^2 = (m_pc^2 + m_ec^2)^2 - m_n^2c^4 < 0.$$

It is possible to see that a real solution is not allowed, and thus p_p (and p_e) cannot be 0.
Supposing $p_n = 0$, it follows that:

$$\begin{aligned}p_n^2c^2 &= (m_pc^2 + m_ec^2)^2 - m_n^2c^4 \\ &= 1.4269MeV^2 > 0\end{aligned}$$

This value represents the smallest p_p such that p_n is minimized to 0. So by inserting this value into the first eq. (1.9), then it follows that below the number density

$$n = \frac{p_p^3}{3\pi^2\hbar^3} = 7.49 \cdot 10^{-9}\text{fm}^{-3}$$

a neutral gas of fermions in chemical equilibrium is a mixture of protons and electrons in equal number density with no neutrons. This condition is the so called *Neutron Threshold*, in which one has

$$p_p = (3\pi^2\hbar^3 n)^{1/3}, \qquad p_e = p_p, \qquad p_n = 0. \tag{1.14}$$

For number densities greater than n_{NT}, from the condition of fixed density it follows

$$p_n = (3\pi^2\hbar^3 n - p_p^3)^{1/3},$$

and putting this equation into the one for the chemical equilibrium, one obtain the following relation in p_p:

$$(m_p^2c^4 + p_p^2c^2)^{1/2} + (m_e^2c^4 + p_p^2c^2)^{1/2} = (m_n^2c^4 + (3\pi^2\hbar^3 n - p_p^3)^{2/3}c^2)^{1/2},$$

which can be solved numerically for p_p and $n(p)$, and thus solutions for pressure and energy density can be found.
Supposing to be in the ultrarelativistic regime, one can ignore all masses in the equation written above and get:

$$\begin{aligned} p_p + p_p &= (3\pi^2\hbar^3 n - p_p^3)^{1/3} \\ 2p_p &= (3\pi^2\hbar^3)^{1/3}(n - n_p)^{1/3} \\ 2(3\pi^2\hbar^3)^{1/3} n_p^{1/3} &= (3\pi^2\hbar^3)^{1/3} n_n^{1/3} \\ 2n_p^{1/3} &= n_n^{1/3} \\ n_p &= \frac{1}{8} n_n. \end{aligned}$$

This represents the asymptotic proton density which is one-height of the neutron density. For this reason it is though that neutron stars, in which the enourmous pressures provide a relativistic regime, are composed mostly of neutrons.

1.5 First NS model and EoSs

The formulas for energy density and pressure given by the previous conditions (Ideal Fermi-gas) were used to build the first NS model by Oppenheimer, Volkoff and Tolman, which assumed a NS as composed of non-interacting relativistic neutrons. Using the properties given by the Fermi model into the TOV equation they found a limiting mass of $\approx 0.72 M_\odot$ and a radius of ≈ 9.6km [12, 13]. After the discovery of pulsars and the measurements of their masses, it became evident that the neutron degeneracy was not sufficient to hold up a NS with $M > 0.7 M_\odot$ and that was necessary to consider even other pressure contributions ([14]). Even if in the real NSs the nuclear forces have to be considered, in order to explain the observed masses $M > 0.72 M_\odot$, the Tolman-Oppenheimer-Volkoff model establishes a value of a NS which is close to a lower bound. The model derived above is described by a so called *soft equation* and it represents a lower limit for equations of state. A further limit is given by another *stiffer equation of state*.
By considering short range repulsion nuclear forces, in addition of degeneracy pressure ones, gravity is more restrained by the resistance of the stellar matter and thus more mass can be supported. Different equations of state describe matter including different contributions that help the pressure gradient. From the relation $v_{sound} = \sqrt{\frac{\partial P}{\partial \rho}}$, where ρ is the density of mass-energy, one can see that each EoS admits different speeds of sound. In a diagram P-ρ, the response of the pressure to the gravity at different densities is shown as a curve. Clearly, for an EoS that describes a stronger pressure resistance, the curve is stiffer, because of, compared to a softer EoS, at the same ρ the pressure is larger. This is why the nuclear repulsive reaction "*stiffens*" the equations of state.
Obviously, any velocity cannot lies the speed of light c, so that by considering an EoS that describes a high density matter in which $v_{sound} = c$, then one obtain an upper limit for EoSs. Such an EoS provides the highest possible resistance of pressure to the gravity and hence implies the maximum mass that can be supported. It shows only a theoretical unrealistic limit, that is called *causality limit*, due to the fact that by crossing the speed of light one would violate the causality principle. In a $P - \rho$ diagram, by considering $c = 1$, this hypothetical limit has a slope $\frac{P}{\rho} = 1$ and any other EoS has to be such that $\frac{\partial P}{\partial \rho} < 1$. The upper bound found by considering $v_{sound} = c$, provides an upper bound on the maximum mass of $\approx 3.2 M_\odot$ ([15]). All EoSs has to be included between these limits, set by causality principle (upper constrain) and by accounting only for the degeneracy pressure (lower constrain). While there is now a pretty large consensus for the EoS of matter in the outer crust, thanks to the fact that similar densities can be obtained in laboratory experiment considering neutron rich nuclei, the available EoSs for the material in the core of a NS are based on models only partially constrained by observations.
Nowadays precise masses for ~ 35 NSs are known, which have values between 1.17 and $2.0 M_\odot$ with radius in the range $10 - 11.5$km [16].

Chapter 2

The Event GW170817

The event GW170817 was a Gravitational Wave (GW) signal detected on 2017 August 17, by the Advanced Laser Interferometer Gravitational-wave Observatory (LIGO) and Virgo network of gravitational-wave observatories. It was the first GW signal for which it was possible to observe even the electromagnetic (EM) counterparts of the event. This unprecendented event provided an important step in astronomy and astrophysics history, becoming a milestone for multi-messenger astronomy and providing insight into dense matter, gravitation and cosmology [17]; furthermore this event provides important clues to understand the origin of short Gamma Ray Bursts (SGRBs) [18].

2.1 Observations

The inspiral and coalescence of a system of binary neutron star (BNS) observed by LIGO and Virgo collaborations [17], was followed by EM emissions. In a time-range of $\sim$ 2s a Gamma Ray Burst (GRB) was observed (GRB170817A) by the Fermi and INTEGRAL satellites. After eleven hours an optical component was detected [19–21] whose properties were consistent with those predicted for a Kilonova emission (KN) [22], an explosion caused by the merging of two dense object and powered by the radioactive decay of heavy elements, which are synthetized during the merger [23, 24]. Radio waves and X-rays have also been detected, roughly two weeks after the event, which can be considered as the products of the interaction between the short GRB and the surrounding medium. More precisely the sGRB jets can produce a shock wave in the environment that generates a delayed broadband synchrotron flash [25].
The observations of EM signals can provide important tools to study the merger product. For instance, the simultaneous presence of different EM components is a consequence of different ejecta materials; in particular, in these case, the two components, an early-time blue one [24] which turned to near-infrared at late time [26, 27] are given by the presence of respectively light and heavy r-process nuclei. The detection of a broadened X-ray to Radio emissions constrained the properties of the surrounding medium and highlighted the properties of the GRB jets (energies, observed angle and collimation; [28]). Moreover, the UV-Optical observations ($1.5 - 9.5$ days after the merge) constrained the two merging objects to be both Neutron Stars.
The observations of the GWs could even clarifies the BNS and its components. These

observations for example provide methods to measure the NS radii, e.g. from tidal effects on the waveform during the end of the inspiral of the BNS (as is explained for example by [29]) or from quasi-periodic oscillations of the remnant of the merger (e.g. [30]), which, however, were not revealed by observations between $\sim$ 10ms and $\leq$ 500s [17].
No precise limit on the maximum NS mass exists for the moment, even if several observations were made in the last years; the only limits on M_{max} are provided by models of the NS mass distribution e.g. [31] or by observation of GRBs e.g. [32].

2.2 Kilonova and GRBs

2.2.1 R-process and Kilonova

The r-process represents a nuclear reaction thought to produce elements heavier than zinc and which require a neutron capture process to form. This process requires large neutron densities, high temperatures and fast timescale, so that the first possible candidate sites are jets of supernova explosions, He-shells in the core collapse of massive stars and BNS mergers. The nuclei synthesized by r-process are radioactive. As the matter expands after the merger, the nuclei decay back to stable ones and the energy released (β-decays) is able to power up a thermal transient known as Kilonova. The properties of KN have been summarized by e.g. [33]. A BNS merger can be followed by two different sources of neutron-rich ejecta [33]. The first one is provided by the ejected matter on the dynamical timescale by shock heating in the merging interface [34], for example, or by tidal forces (e.g. [35]). While the shock-heated material expands along the polar direction and has an electron fraction $Y_e \gtrsim 0.25$ [36], the tidal matter emerges in the orbital plane of the binary system and possesses a lower electron fraction $Y_e \lesssim 0.1 - 0.2$.
The second source of ejecta is given by the outflowing material from the accretion torus around the remnant. These outflows possess an electron fraction in the range $0.1 - 0.5$, and it increases due to the neutrino irradiation of the ejecta [37].
The KN that followed the event GW170817 showed two different ejecta components (respectively semi-relativistic and non-relativistic). The earliest and blue one ($\lesssim$ 2 day) requires an ejecta mass of $M_{ej}^{blue} \approx 0.1 \cdot 10^{-2} M_\odot$ of lanthanide free material ($Y_e \gtrsim 0.25$) and a velocity of $v_{ej}^{blue} \approx 0.2 - 0.3c$ [38]. The second emission, red and at later times, requires instead $M_{ej}^{red} \approx 4 - 5 \cdot 10^{-2} M_\odot$ of material with $Y_e \lesssim 0.25$ and velocities $v_{ej}^{red} \approx 0.1 - 0.2c$ [39].
Thus the total energy of KN ejecta observed results to be:

$$E_{kin} = \frac{M_{ej}^{blue} v_{ej}^{blue2}}{2} + \frac{M_{ej}^{red} v_{ej}^{red2}}{2} = 1.0 \cdot 10^{51}\,\text{erg}.$$

The UV and Optical observations of the ejecta and their inferred properties provided constraints for the merger objects [38]: the ejecta characteristics (especially the velocity) indeed were such that to have dynamical origin that can be supported by a shocked interface [40]. In the case of a BH-NS merger, there would not be a contact interface, so that the high electron fraction inferred for the blue ejecta could only be provided by outflows from the accreting disk [41].

2.2.2 GRB

A GRB is a very intense flash of γ-rays, which can be distinguished in two classes on the basis of its duration. The long GRB are produced by collapsars [42], rapidly rotating $\geq 30M_{\odot}$ Wolf-Rayet stars, and represent the dominant population. They have a peak around $\sim$ 30s and a soft spectrum. On the other hand the short GRBs are spectrally harder, they have a peak at $\sim$ 1s and are generated by compact binary mergers [43, 44].
The observations of the merger GW170817, however, revealed an amount of energy radiated away and, in the case in which kinetic energy originates from an on-axis GRB jet, a kitetic energy lower than those of short cosmological GRBs by several orders of magnitude [17, 44, 45]. It was thought this is because the GRB was observed well outside of its core. Indeed the delayed sinchroton X-ray and radio emission, revealed two weeks later, result to be quite consistent with the afterglow of a more powerful jet ([25, 28] respectively for X-ray and radio detection). The kinetic energy inferred for an off-axis GRB is $E_{GRB} \lesssim 10^{50}$erg [25, 28], which is in the range of short cosmological GRBs [46].
The production of GRB narrows the range of the possible merger remnants; indeed the observation of such a jet could indicate the presence of a BH. As Murguia Berthier et al. [47] have shown, the gravitational collapse cannot be considerably delayed ($\leq$ 100ms) before the outflow is dissolved. In this case the GRB's delay after the merger implies that the remnant underwent prompt collapse or formed a short-lived Hypermassive or Supramassive NS. There would be the possibility that a long-lived magnetar was produced by merger, as the late-time X-ray seem to show, but GW170817 did not show evidence for such a signal [17].

2.3 Constraints on the Remnant

Even if the maximum mass value is not known yet, it plays a very important role in the NS properties. For instance it affects the binary merger product (BMP) and the emitted EM signals. Indeed the KN observed signals depend upon the remnant (Fig. 2.1). Thus the problem of understanding what the merger produced is important to constrain the maximum NS mass. In fact the ability of the merged object to be stable against gravity is strictly correlated to the maximum mass that can be sustained against collapse. Furthermore from the value of the remnant mass it is possible to constrain the properties of EoS [18].
By defining a threshold mass of the total binary mass $M_{th} \approx kM_{max}$ (M_{max}: maximum gravitational mass), where $k \approx 1.2 - 1.6$ is a proportionality factor, which increases for lower values of the compactness of a NS ($C_{max} = \frac{GM_{max}}{c^2 R_{1.6}}$ where $R_{1.6}$ is the radius of a $1.6M_{\odot}$ NS; Sec. 2.4.3 [34]), the different scenarios are divided by different mass ranges. For a BNS with $M_{tot} > M_{th}$ the BMP will undergo prompt collapse to a black hole on the dynamical-timescale [48, 49]. For smaller value of M_{tot} the merger will produce a hypermassive neutron star (HMNS), whose differential rotation can sustain it against an immediate collapse. If the BNS has a mass $M_{tot} \lesssim 1.2M_{max}$, then the merger remnant will be a supramassive neutron star (SMNS), which can be stable, for more than several seconds, even if its differential rotation is removed, that should happen roughly $\lesssim 10 - 100$ ms [50–52]. More correctly, a SMNS can be stable against its own gravity until its rigid body angular momentum is removed (e.g. through magnetic spin-down). Finally, a BNS can produce an indefinitely stable NS remnant if $M_{tot} \lesssim M_{max}$ [53, 54].

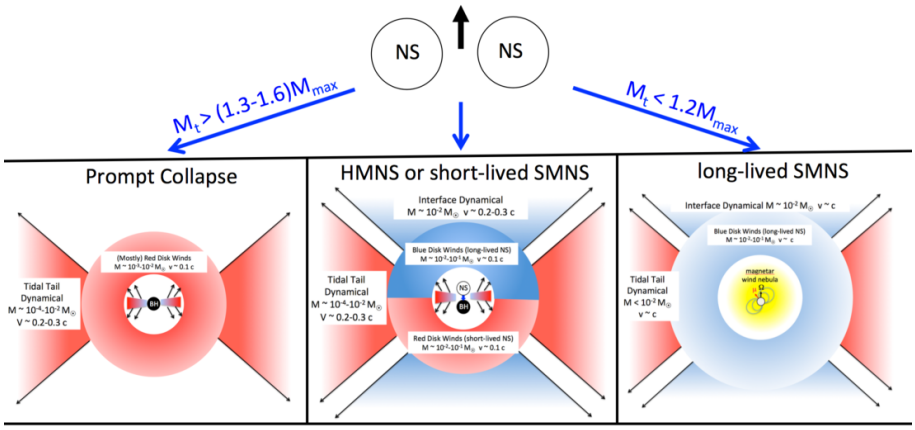

Figure 2.1: This figure shows three possible BNS merger remnants, which depends upon the total mass of the system. The different type of ejecta are also reported. For a prompt collapse to a BH the larger contribution to the ejected material is given by tidal forces, that power the KN, while other matter outflows from the red torus. The intermediate case produces both blue and red KN ejecta with semi-relativistic velocities. In the last case the merger imparts relativistic expansion speeds to the KN ejecta [22].

For the BNS merger GW170817, the quantity of blue ejecta revealed disfavours the possibility of a prompt collapse to a BH. Indeed, from GR numerical simulations, it derives that a prompt collapse could eject only a small quantity of material from the merger interface ($\lesssim 10^{-4} - 10^{-3} M_\odot$, [49]), which is inconsistent with the data inferred ($M_{ej}^{blue} \gtrsim 10^{-2} M_\odot$). In principle there could be another source of ejecta that can contribute: the outflows from the torus. However the winds of the ejecta required for a blue KN signal (Sec. 2.2.1) represents a small part of the initial accretion disk, that in addition is small for a prompt collapse [55, 56]. Moreover the velocities predicted by Fernandez et al. [57] for the disk winds are lower than those inferred for the blue KN component observed. A HMNS could be an appropriate remnant because its longer lifetime (10 ms) allows it to produce more ejecta than a prompt collapse. Like BNS merger simulations [58] show, the velocity and the mass of ejecta of both blue and red components inferred from GW170817 are consistent with those expected after the collapse of a short-lived HMNS. A long-lived SMNS or a stable NS are also disfavored of course by the presence of short GRB [47], but even because of the amount the kinetic energy observed.
A supramassive NS possesses a large quantity of rotational energy $T \approx 10^{53}$ erg, which can be deposited around the compact object after the merger, promoting the collapse of the object. The extractable rotational energy is expressed as $\Delta T = T_0 - T_o$ [22], where T_0 represents the energy that a SMNS possesses immediately after that differential rotation has been removed, and T_o is the rotational energy when collapse occurs. Margalit and Metzger (2017) took T_0 equal to the rotational energy which approximates the state of the merger product when it loses its differential rotation configuration [22]. In Fig 2.2 the pace of ΔT for the different remnants is shown. For a SMNS the most appropriate methods that can removes ΔT, allowing its collapse, is the extraction of angular momentum through magnetized jets, which are generated in the remnant [59].
By indicating the rate of the energy removed by magnetic jets as

$$\dot{E}_{mag} = \frac{\mu^2 \Omega^4}{c^3}(1 + \sin^2 \chi),$$

where $\mu^2 = B_d R_{NS}^3$, B_d, $\Omega = 2\pi/P$ and χ are the dipole moment, the strength of the surface magnetic dipole, the rotational velocity and the angle between the dipole and rotation axis, and by taking $R_{NS} = 12$km and $\chi = 0$, one obtain the timescale for the energy removal as:

$$\tau_{er} = \frac{\Delta T}{\dot{E}_{mag}} = 24\,\mathrm{s}\left(\frac{\Delta T}{10^{52}\,\mathrm{erg}}\right)\left(\frac{B_d}{10^{15}\,\mathrm{G}}\right)^{-2}\left(\frac{P}{0.8\,\mathrm{ms}}\right) \tag{2.1}$$

By requiring that collapse occurs on $\tau \lesssim 2$ s after the merger consistently with the GRB, then SMNS would be such that $B_d \gg 10^{15}$G or $\Delta T \ll 10^{53}$erg. This precludes the possibilities for the remnant to be a stable NS or a long-lived SMNS ($\Delta T \approx 10^{52} - 10^{53}$erg). It would possible to argue that a SMNS can also spin-down through the emission of GW, so that the remnant can lose energy through non electromagnetic detectable signals; this would imply an enhancement of the energy released into the environment [60, 61](a raise of the red dashed line in Fig. 2.2). However, this could happen only if the interior toroidal magnetic field exceeds the external poloidal one by a factor of $\gtrsim 100$, which represent an instability condition [62], and, first of all, it requires a much longer collapse time ($\tau \gtrsim 100$ s). Thus this picture results inconsistent with the observation (especially with the after merger GRB observation time).
From all kind of observations and predictions it follows that the more consistent merger remnant results to be a HMNS or a short-lived SMNS.

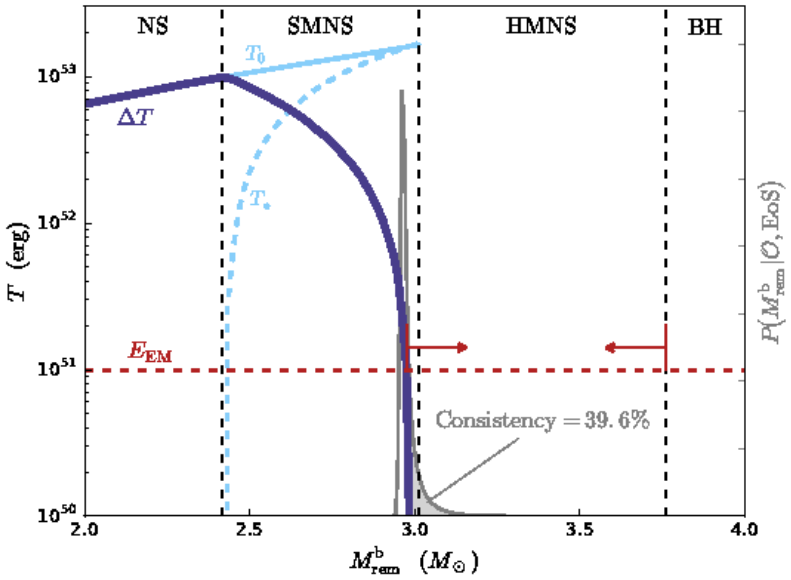

Figure 2.2: The pace of ΔT [22]: the red dashed line represents the energy inferred from EM signals of GW170817, while the black dashed ones correspond to the boundaries between the different remnant types. The constraints given $\Delta T \gg E_{EM}$ and the considerations reported in the text allow the remnant to belong to the red arrows delimited range. It is possible to note that, as it was underlined in this section, $T_o = T_0$ in the boundary between SMNS and HMNS. It highlights that a HMNS cannot avoid collapse without a differential rotation.

2.4 Constraints on NS properties

2.4.1 Quasi-universal Relations

In order to constrain the properties of a NS, for example its maximum mass in a non-rotating configuration (and thus the properties of the EoSs), one can use some universal relations, i.e. equations that are quite largely independent of the EoSs. Some of these have been shown by Yagi & Yunes ([63]) (for example between the moment of inertia and the quadrupole moment). An example of universal relation is that between the maximum mass of an uniformly rotating NS and M_{TOV}(Sec. 1.3). It results that, for each EoS used, M_{max} is $\sim 20\%$ larger than the maximum mass that a non-rotating NS can support: $M_{max} = 1.20^{+0.02}_{-0.02} M_{TOV}$ [64]. Even other authors confirmed this universal relation (e.g. [65]).
Another important quasi-universal relation connects gravitational mass (M^g) to the baryonic one (M^b). The value of the ratio between them, fixed in the configuration in which the gravitational mass is equal to the maximum sustainable mass, is only weakly dependent of the EoS specified; every EoS studied implies a ratio value within $\lesssim 2\,\sigma$ (Fig. 2.3). The value obtained and its standard deviation are:

$$\eta := \frac{M^b}{M^g_{max}} \simeq 1.171, \quad \sigma = 6.8 \cdot 10^{-3} \tag{2.2}$$

This value, as shown, represents for the moment the most accurate estimate for the baryonic-to-gravitational mass ratio, indeed it has a larger consistence than the Timmes relation, which are shown for different EoSs as dashed line (Fig 2.3) [66].

2.4.2 Constraints on NS masses

Proceeding to constrain the maximum NS mass, one can assume that the post merger system can be described by the initial total mass. In a scenario in which the remnant is born with a differential rotation and evolves ejecting material and losing rotational energy (Sec. 2.3), the total mass can be considered as the sum of the ejected baryon mass M^b_{ej} from the core of the remnant, the initial baryon remnant's mass M^b_{rem} and the baryon mass of the uniformly rotating core $M^b_{core}(t) = \xi M^b_{rem}$.
By considering the baryon mass conservation, then $M^b_{core}(t_0) = M^b_{core}(t) + M^b_{ej}(t)$. Now, it can be assumed that the remnant becomes uniformly rotating in the vicinity of the maximum mass. This can be justified by the fact that even if a SMNS can be stable without differential rotation, the constraints given by EM signals imply that the remnant has to collapse ($M \gtrsim M_{max}$) quite quickly ($\lesssim$ 2s). So one has:

$$M^b_{core}(t_{collapse}) = M^b_{max}.$$

Thus:

$$\begin{aligned} M^b_{core}(t_{collapse}) = M^b_{max} &= M^b_{core}(t_0) - M^B_{ej}(t_{collapse}) \\ &= \xi M^b_{rem} - M^b_{ej}(t_{collapse}) \end{aligned}$$

Now, by considering the universal relations $M_{max} = \chi M_{TOV}$ and $M^b_{max} = \eta M_{max}$, with $\chi = 1.15$ to avoid the error of considering the remnant exactly in the maximum mass limit [64], it follows that:

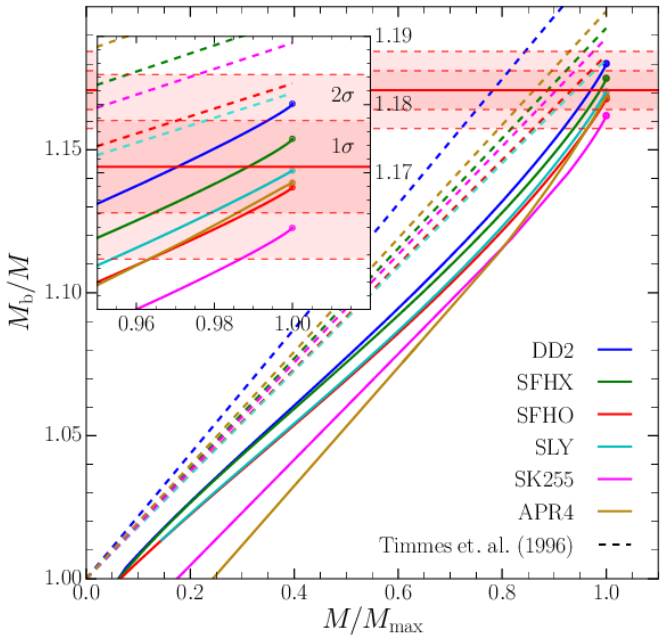

Figure 2.3: The quasi-universal relation between M^b and $M = M^g$ is shown [18]. In the point in which $M = M_{max}$, for each EoS considered, $\eta \simeq 1.171^{2\sigma}_{2\sigma}$. The dashed line represent the Timmes relation $M^b/M = 1 + 0.75M$ [66].

$$M_{TOV} = \chi^{-1} M_{max} = \chi^{-1}(\xi\eta^{-1} M^b_{rem} - \eta^{-1} M^b_{ej}) \\ = \chi^{-1}(\xi M^g_{rem} - \eta^{-1} M^b_{ej})$$

where $M^g_{rem} = \eta^{-1} M^b_{rem} = 2.74^{+0.04}_{-0.01} M_\odot$, which is consistent with low spin priors [17, 18] and $\xi = 0.95^{+0.06}_{-0.06}$ is the mass fraction of the core after dynamical ejection [67]. In order to estimate the mass of the ejecta one can use standard KN models [68], to obtain: $M^{blue}_{ej} = 0.014^{+0.01}_{-0.01} M_\odot$ (as reported in Sec. 2.2.1).
From the last written equation and data inferred it follows that the maximum mass which can be supported against gravity of a neutron star with no rotation is in the range

$$2.01^{+0.17}_{-0.16} M_\odot \lesssim M_{TOV} \lesssim 2.16^{+0.17}_{-0.15} M_\odot \tag{2.3}$$

where the lowest limit is given by the observations of a binary system pulsars [69] and the asymmetric errors are given by computing the standard deviation for the upper and lower limit separately in M_g and χ because of the values near to the upper and lower limit are not equally favourite [18].

However some assumptions are not completely justified; for instance the fact that the creation of a GRB implies that a BH formed, which remains unclear, or even that the BH can follow only by a prompt collapse or a HMNS remnant.
Another way to proceed to determine a maximum mass limit, without considering the

Timmes relation or an universal value for ξ, and also moving away from assuming that GRB implies that a BH formed, was given by Margalit & Metzger [22] through the use of RNS code [70] to construct General Relativistic equilibrium NS models for different EoSs. For each EoS the range of GW170817 measured gravitational mass can be translated into the analogous baryonic mass, using the probability distribution function:

$$p(M^b_{rem}|\Theta, EoS) = \int dM^b_1 \int dM^b_2 \delta(M^b_1 + M^b_2 - M_{ej} - M^b_{rem}) \cdot \\ \cdot p(g_{EoS}(M^b_1), g_{EoS}(M^b_2)|\Theta)|g'_{EoS}(M^b_1)||g'_{EoS}(M^b_2)| \tag{2.4}$$

where EoS acts in converting baryonic and gravitational masses ($M^g = g_{EoS}M^b$), the function $p((M^g_1),(M^g_2)|\Theta)$ is the probability distribution function of NS gravitational masses obtained by the BNS waveform Θ [17] and δ is the Dirac function that, in this case, fixes the value of the sum M^b_{rem}, reflecting the law of mass conservation, since $M_{ej} \simeq 2 \cdot 10^{-2} M_\odot$ as given by observations. For all EoSs considered one has to compare the derived mass of the remnant with the allowed range of possible baryonic masses S, fixed between the maximum mass that can avoid a prompt collapse ($M^b_{rem} \leq M_{th}$; [34]) and the minimum mass which results in a SMNS with ΔT less than the upper limit inferred by the KN observation ($E_{EM} \lesssim 10^{51}$erg; Fig. 2.2). Then, by integrating (2.4) over this fixed mass range, it can be obtained the probability of the range S, i.e. the probability that, for a chosen EoS, the mass of the remnant belongs to S. This probability can be seen as the "consistence" between the inferred data and the predictions of the EoS used [22]:

$$P(M^b_{rem} \in S, EoS) = \int_S p(M^b_{rem}|\Theta, EoS) dM^b_{rem} \tag{2.5}$$

In Fig. 2.2, an example of this procedure is shown. From this analysis a new formulation for an approximate criterion follows. For all EoSs, it results indeed that $M^b_{SMNS} \approx 1.18 M^b_{max}$, [22], thus it is possible to establish that for the maximal non-rotating NS mass, consistent with the event:

$$M^b_{max} \lesssim M^b_{rem}/\xi, \tag{2.6}$$

with $\xi \simeq 1.16 - 1.21$.
Finally, by weighting the EoSs with values of M^g_{max} under the limit $2.01 M_\odot$ in the previous calculation (2.5) for a better consistency with the maximum mass measured [69], the final results for a maximum gravitational mass of a non-rotating NS results to be (at 90% confidence)

$$M_{TOV} \lesssim 2.17 M_\odot. \tag{2.7}$$

It is a result completely consistent with the one inferred with the previous method. This is a big result because it represents a quite reliable constrain, since both GR simulations or fits of formulas fixed by numerical simulations and simple arguments from kilonova modeling lead to this value.

2.4.3 Constraints on NS radii

The measurements of the NS radii have progressed through the past years and many techniques have been devised. The most common methods are observations quasi-periodic oscillations during the accretion of a NS, asteroseismology, Pulsar glitches [16] and, as it was written in Sec. 2.1, characteristics of the waveform of the detected gravitational waves. With the observation of the event GW170817, a new method was proposed by Bauswein et al. [71].

The total mass of the BNS, if it avoided a prompt collapse, provides a lower limit on the threshold mass. Indeed, as discussed before, M_{th} has to be $< kM_{max}$ in order to avoid undergoing an immediate collapse. Thus, from the moment that the previous discussion has constrained the remnant to be a HMNS, one can consider the total mass of the BNS as less massive than the threshold one:

$$M_{th} > M_{tot} = 2.74^{+0.04}_{-0.01} M_{\odot}. \tag{2.8}$$

The threshold mass of the BNS is dependent on the EoS. However it was found [34], by considering different types of EoSs that M_{th} quite accurately follows the relations

$$M_{th} = \left(-3.606 \frac{GM_{max}}{c^2 R_{1.6}} + 2.38\right) M_{max} \tag{2.9}$$

$$M_{th} = \left(-3.38 \frac{GM_{max}}{c^2 R_{max}} + 2.43\right) M_{max} \tag{2.10}$$

which have been semi-analytically confirmed [72] (the first equation shows a very good accuracy: $\lesssim 0.1 M_{\odot}$). There are now two way to proceed: one can use the limit set by eq. 2.8 or consider more properties of the remnant, in order to obtain a better limit for M_{th} and so to more strictly constrain the NS radii. Starting from the first way, equations 2.9 and 2.10, with the easily set limit for M_{th} yield the NS radii $R_{1.6}$ and R_{max} constraints reported in Fig. 2.4.
In order to obtain constraints for $R_{1.6}$ through the relation 2.9, one has to fix the M_{max} values. By considering the EoSs as maximally stiff ($v_{sound} = c$), then one can fix an upper limit for M_{max} of a $R_{1.6}$ NS ($M_{max}(R_{1.6}) < \frac{1}{3.10} \frac{c^2 R_{1.6}}{G}$) and thus obtain an equation in the single $R_{1.6}$ variable. Hence, by substituting the expression of $M_{max}(R_{1.6})$ into eq. 2.9, it follows:

$$M_{th} = \left(\frac{-3.606}{3.10} + 2.38\right) \frac{1}{3.10} \frac{c^2 R_{1.6}}{G} > 2.74 M_{\odot}$$

from which the two constraints below follow:

$$M_{th} \geq 1.22 M_{max}, \quad R_{1.6} \geq 10.30^{+0.15}_{-0.03} km \tag{2.11}$$

where the error bars are given by the errors in M_{tot}.
With the same procedure ($M_{max}(R_{max}) < \frac{1}{2.82} \frac{c^2 R_{max}}{G}$), for a NS with M_{max} it follows that:

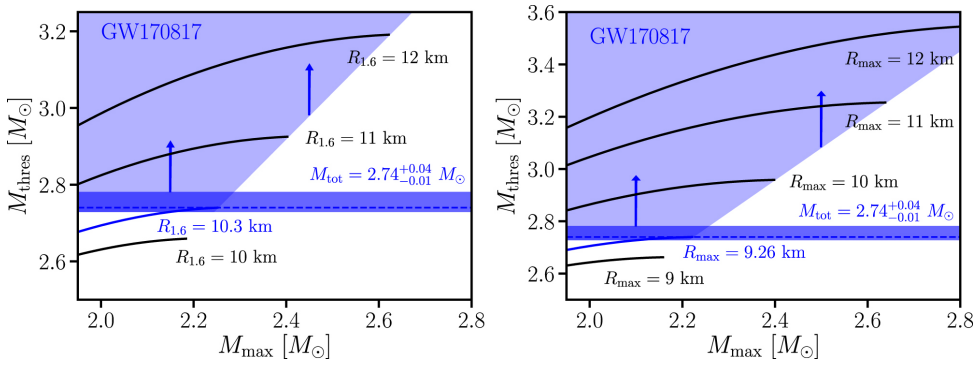

Figure 2.4: The constraints on radius obtained by Bauswein et al. [71]. On the left panel $R_{1.6}$ is shown whereas in the other one panel the radius of a maximum mass NS is reported. The large dark blue line represents the mass of the merger M_{tot}, and in both figures the smallest radius allowed is symbolized in blue. The two big light blue areas represent the allowed radii.

$$M_{th} \geq 1.23 M_{max}, \quad R_{max} \geq 9.26^{+0.17}_{-0.03} km. \tag{2.12}$$

In Fig. 2.4 $M_{th}(M_{max}; R_{1.6})$ and $M_{th}(M_{max}; R_{max})$ are represented for different values of $R_{1.6}$ and R_{max} respectively as black lines that terminate at the value of the maximum mass fixed by causality.

By following the second possibility, instead of using the limit 2.8, it is more realistic to assume an at least 10ms stable remnant, which is compatible with the GW170817 inferred properties [22,38,40]. Numerical simulations of Bauswein et al. [71] show that, in the case considered $M_{th} - M_{tot} \geq 0.1 M_\odot$. Proceeding like above, this value for the threshold mass given

$$R_{1.6} \geq 10.68^{+0.15}_{-0.04} km \quad R_{max} \geq 9.60^{+0.14}_{-0.03} km. \tag{2.13}$$

This way to constrain the NS radii results to be quite robust because it is based only on a well measured M_{tot}, on a single empirical relation (Eq. 2.9-2.10), semi-analytically supported, and on the clearly and likely hypothesis that there were not a prompt collapse (Sec. 2.3). This method is also base on a conservative assumption, i.e., assuming an equal-mass BNS merger. Indeed in a different situation one would have a reduction of the threshold mass (and hence of R), because, at fixed M_{tot} and NS-NS distance, an asymmetric-mass system have less angular momentum, and thus a lower stabilization. Through the analysis of five representative EoSs was verified that BNS mergers with $q = M_1/M_2 = 0.6$ have a lower M_{th} compared to equal mass ones ($q = 1$; [71]).

2.5 Constraints on EoSs

Although several theoretical and experimental studies have been developed, the problem of understanding the behaviour of very dense matter is still unresolved. Due to the fact that densities $\gtrsim 10^{14}\text{gcm}^{-3}$ cannot be reached in laboratories, astrophysical observations and modelling are the only approaches that can be followed to shed light on this issue.
As discussed in the first chapter, given the TOV equation, the Equation of State of NSs matter determines the properties of such stars, especially their masses and radii. Astrophysical observations can be used to infer the EoS. Indeed the mass-radius (M-R) relation can be used to constrain the EoS. This is for instance what one can inferred by the constraints found for M_{TOV}. Through the years many techniques have been improved that permit to combine measurements on radius with constraints on the maximum mass. Furthermore various universal relations have been found between different properties of NSs, which allow to fix limits on the characteristics of such objects and thus to favour some EoSs and disfavour others, according to their predictions.
With the event GW170817 some constraints on NSs properties have been inferred and thus it allowed to refine the characteristics of such compact objects, permitting to have a better reading of the high-density matter equation of state. From the methods followed in the previous sections, some EoSs constraints have been inferred. For instance, using the quasi-universal relation derived by Rezzolla et al., has been set a constrain on the maximum mass that disfavours an EoS usually very used in numerical-relativity simulation (DD2; [18]), whereas favours others which have maximum masses $\lesssim 2.1M_{\odot}$.
With the procedure that moves away from assumption on the merger remnant, supported by the use of numerical simulations (RNS code), it has been found a M_{TOV} limit that strongly rules out very stiff EoSs (MS1, MPA1, ENG) while promotes softer equation with $M_{TOV} \lesssim 2.1 - 2.2M_{\odot}$ [22]. In Table 2.1 it is possible to see the EoSs considered in this methods, with their consistency with the results inferred by GW170817 given by the relation 2.5. The three stiffer equations, for example, provided a quantity of energy ΔT that was largely inconsistent with one inferred by the merger. The last four ones are marked with an "a" because of they allow a maximum mass that is inconsistent with the highest NS mass nowadays known ($2.01 \pm 0.04M_{\odot}$).
Even from the constraints on neutron stars radii EoS limits derive. In Fig. 2.5 are shown some M-R relations provided by different equations of state. One can see that while with the constraints set by considering the limit $M_{th} > 2.74M_{\odot}$(red boxes) only one EoS has been ruled out, with the more realistic second way (purple boxes) three different equations have been disfavoured. Indeed, for example, these admit too short radius for a NS of $1.6M_{\odot}$. The radius limits obtained exclude EoS models describing very soft nuclear matter, which due to the softer reaction of the pressure to the gravity allow smaller radii. However, it was checked with numerical simulations that a binary neutron stars described with such NSs would underwent a prompt collapse [71].

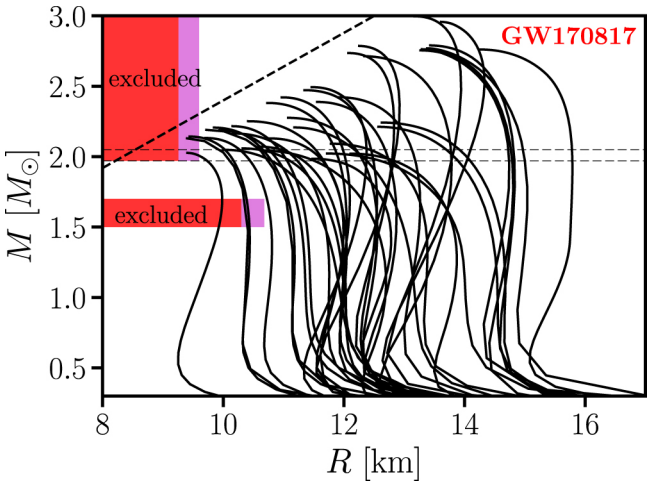

Figure 2.5: Mass-radius relations given by different considered EoSs. The red areas represent the exclusion regions given by the limit on the threshold mass, while the purple ones are obtained by considering the more realistic situation of a delayed collapse ($\gtrsim$ 10ms). The dashed bigger shows the limit set by causality, while the horizontal ones report the maximum NS mass measured [71].

EoS	$M^g_{max}(M_\odot)$	$R_{1.3}$(km)	$M^g_{SMNS}(M_\odot)$	$\Delta T_{max}(10^{53}$erg)	Consistency (%)
MS1	2.77	14.9	3.31	1.8	0.0
MPA1	2.45	12.4	2.97	1.8	0.0
APR3	2.37	12.0	2.84	1.7	0.2
ENG	2.24	12.0	2.67	1.4	5.2
WFF2	2.20	11.1	2.63	1.6	10.2
APR4	2.19	11.3	2.61	1.5	18.4
SLy	2.05	11.8	2.43	1.2	100.0
H4	2.02	14.0	2.38	0.8	100.0
ALF2	1.98	12.7	2.41	0.9	100.0
GNH3[a]	1.96	14.3	2.29	0.7	100.0
ALF4[a]	1.93	11.5	2.35	1.0	99.8
BBB2[a]	1.92	11.2	2.27	1.1	99.4
MS2[a]	1.80	14.3	2.10	0.6	99.9

Table 2.1: EoS properties and their consistencies in percentage [22]. The apex "a" indicate that the model of equation of state is ruled out due to the inconsistency of its maximum mass with the current observations [69].

Chapter 3

Conclusions

The recap of the results inferred by the event GW170817 illustrates different way that have been used to constrain firstly the properties of NSs and then the equations of state. Approximately the same results on maximum masses have been derived with two different proceeds. One is supported only by analytical universal and quasi-universal relations and by the simple assumption consisting into considering the post merger remnant as a SMNS. The other one followed method, instead, doesn't lean on assumptions, for instance on the need to have a collapse to BH to explain GRB emissions, or in the remnant object. However the GR magnetohydrodynamical simulations of Ruiz et al. [73] also favour a scenario in which the remnant has a mass above supramassive limit but below the critical threshold (thus, in which the remnant was a HMNS). The only assumption followed is that the remnant didn't collapse immediately after the merger. Even the properties of GRB were not taking in account, because of the characteristics of GRB170817A are peculiar and can point a difference between this one and the common short GRBs [22]. The only consideration that has been used concerns the amount of energy inferred by observations $\Delta T \lesssim 10^{51}$erg and the calculated M_{tot} of the BNS with which a range on M^g_{rem} was fixed. The new method proposed by Bauswein et al. to constrain the NS radius are also very general, furthermore, overall conservative. Even whit this procedure the total mass of BNS has been taken into account and during the calculations strictly hypothesis have been avoided (e.g. it has been considered a mass symmetric BNS). It is a promising way to constrain the high density EoSs due to its simple assumptions. However, all the methods used can be refine and improved.
The relations 2.9 and 2.10 can be further corroborated given stronger M_{th}-M_{max} relations and more precisely radius measurements, for example with the detection of a long-lived SMNS merger remnant one could tightly constrain the radius, due to the fact that longer the lifetime is, more the difference between M_{th} and M_{tot} is large [71]. Even through future observations some results will be better explained and refined, especially for the relation which concern kilonova and GRBs. Some assumptions employed could be only partially true, for instance maybe in the amount of the energy imparted by the remnant an additional part was missed [22], or, as it was reported in Sec. 2.3, some of this energy can be lost through GW emissions. Even if there are no evidence of such signals, the sensitivity of the detectors decreases at high frequencies and this can limit the constraints given for the energy amount.
The analysis on the maximum mass neglects also the thermal pressure on the stability of the merger remnant. This pressure contribution can support the remnant against gravity and thus providing an increase of its maximum mass ad lifetime while induces a decreasing

of its density. This larger life can allow cooling or others forms of energy loss driving the merger product on an unstable configuration, which implies a reduction of the gravitational mass [74]. Thermal pressure in a SMNS outer layers can reduce its M_{max} by up to 8%, that can weaken the constraints inferred in the previous sections [22].
Of course the NS properties will be able to be constrained in a better way with future experiments and improvements of theories and simulations; this is the first time that GW and EM signals could have been unified to understand an astrophysical event such a BNS merger. For example, the recent discovery of the Millisecond Pulsar J0740+6620 by Thankful Cromartie et al. (2019, [75]) would be used to better constrain the maximum gravitational mass. This pulsar, with its mass of $2.14^{+0.10}_{-0.09}M_{\odot}$, represents the most massive neutron star ever observed [75]. This value can be used to discard EoSs which have been accepted till now and that predict a maximum gravitational mass below this value. Furthermore in the method proposed by Margalit & Metzger (Sec. 2.4), the considered EoSs which predicted a mass below $2.01M_{\odot}$ [69] have been weighted. Thus, with this new upper observed limit, a better approximation could be found.
These results show how the astrophysical approaches are useful to investigate the high density matter and to obtain constraints on its behaviour, which is impossible to study in terrestrial laboratories.

Appendices

Appendix A

Calculations

Integrals for Ideal Fermi-gas EoS

From the relations (1.8), one has, e.g., for the pressure: $A = \frac{c^2}{3\pi^2\hbar^3}$,

$$P(p) = A\int_0^p \frac{p^4}{\sqrt{p^2c^2+m^2c^4}}dp = A\int_0^p \frac{1}{mc^2}\frac{p^4}{\sqrt{\frac{p^2}{m^2c^2}+1}}dp =$$
$$= Am^4c^3\int_0^{\eta_0}\frac{\eta^4}{\sqrt{\eta^2+1}}d\eta$$

where $\eta = \frac{p}{mc}$, so that $dp = mcd\eta$. Thus, integrating by parts

$$Am^4c^3\int_0^{\eta_0}\frac{\eta^4}{\sqrt{\eta^2+1}}d\eta = Am^4c^3\left(\sqrt{\eta_0^2+1}\eta_0^3 - \int_0^{\eta_0}3\eta^2\sqrt{\eta^2+1}d\eta\right)$$

Now, by putting $\eta = \sinh x,\ d\eta = \cosh x dx,\ \eta_0 = \sinh x_0$ and $B = Am^4c^3\sqrt{\eta_0^2+1}\eta_0^3$ from the relation $\cosh^2 x = 1 + \sinh^2 x$, the integral left unsolved becomes

$$P = B - 3Am^4c^3\int_0^{\eta_0}\sinh^2 x\cosh^2 x dx =$$
$$= B - 3Am^4c^3\left(\int_0^{\eta_0}\sinh^2 x dx + \int_0^{\eta_0}\sinh^4 x dx\right)$$

so, integrating again by parts each integral components one obtain

$$P = B - 3Am^4c^3\left(\frac{1}{8}\sinh x\cosh x + \frac{\cosh x\sinh^3 x}{4} - \frac{1}{8}x\right).$$

By making the inverse substitutions one finally obtains

$$P(p) = \frac{m^4c^5}{3\pi^2\hbar^3}\left(\frac{\mu p^3}{m^4c^5} - \frac{3}{2}\frac{\mu p}{m^2c^3} + \frac{3}{2}\ln\left(\frac{pc+\mu}{mc^2}\right)\right) =$$
$$= \frac{1}{12\pi^2\hbar^3}\left[\frac{\mu p}{c^2}\left(\mu^2 - \frac{5}{2}m^2c^4\right) + \frac{3}{2}m^4c^5\ln\left(\frac{pc+\mu}{mc^2}\right)\right]. \tag{A.1}$$

Lagrangian Multipliers

Theorem: let $f(x_n)$, $n = 1, 2, 3$, be a function of x_n variables and let M be a differential variety (with dimension $n - m = 3 - 2 = 1$) that describes the ker of a function $g(x_n) = (g_1, g_2)$. A point $x \in M$ is a stationary point for $f \iff \nabla f(x)$ is generated by the $n - m$ gradients $\nabla g_1(x), \dots, \nabla g_{n-m}(x)$, thus $\iff n - m$ real numbers $\lambda_1, \dots, \lambda_{n-m}$ exist such that

$$\nabla f(x) = \lambda_1 \nabla g_1(x) + \cdots + \lambda_{n-m} \nabla g_{n-m}(x),$$
$$g(x_n) = 0.$$

In the case of the energy of an ideal Fermi-gas with fixed baryon density and charge neutrality, it is possible to see M as the variety fixed by the two conditions $g_1 = n_e - n_p = 0$ and $g_2 = n - n_p - n_n = 0$ (e.g. a curve in $((n_n, n_p, n_e)$ space) and $\epsilon(n_n, n_p, n_e)$ as the function of which one wants to calculate the minimum point. Thus:

$$\begin{cases} \frac{\partial \epsilon}{\partial n_n} = a \frac{\partial g_1}{\partial n_n} + b \frac{\partial g_2}{\partial n_n} = -b \\ \frac{\partial \epsilon}{\partial n_p} = a \frac{\partial g_1}{\partial n_p} + b \frac{\partial g_2}{\partial n_p} = -a - b \\ \frac{\partial \epsilon}{\partial n_e} = a \frac{\partial g_1}{\partial n_e} + b \frac{\partial g_2}{\partial n_e} = a \\ n_e - n_p = 0 \\ n - n_p - n_n = 0 \end{cases}$$

From the chain rule it follows

$$\frac{\partial \epsilon}{\partial n} = \frac{\partial \epsilon}{\partial p} \frac{\partial p}{\partial n}$$

with $\frac{\partial \epsilon}{\partial p} = \frac{1}{\pi^2 \hbar^3} \sqrt{p^2 c^2 + m^2 c^4} p^2$ and $\frac{\partial p}{\partial n} = \left(\frac{1}{\pi^2 \hbar^3} p^2\right)^{-1}$, so that

$$\begin{cases} \frac{\partial \epsilon}{\partial n_n} = \sqrt{p_n^2 c^2 + m_n^2 c^4} = -b = \mu_n \\ \frac{\partial \epsilon}{\partial n_p} = \sqrt{p_p^2 c^2 + m_p^2 c^4} = -a - b = \mu_p \\ \frac{\partial \epsilon}{\partial n_e} = \sqrt{p_e^2 c^2 + m_e^2 c^4} = a = \mu_e \end{cases}$$

where μ is the chemical potential. From this follows the condition for the existence of a stationary point:

$$\mu_n = \mu_p + \mu_e \tag{A.2}$$

Bibliography

[1] L. D. Landau, "To the Stars theory," *Phys. Zs. Sowjet., vol.1, p.285, 1932 (English and German)*, vol. 1, p. 285, Dec. 1932.

[2] W. Baade and F. Zwicky, "Remarks on Super-Novae and Cosmic Rays," *Physical Review*, vol. 46, pp. 76–77, July 1934.

[3] A. Hewish, S. J. Bell, J. D. H. Pilkington, P. F. Scott, and R. A. Collins, "Observation of a rapidly pulsating radio source," *Nature*, vol. 217, pp. 709–713, 1968.

[4] A. Hewish and S. E. Okoye, "Evidence for an unusual source of high radio brightness temperature in the crab nebula," *Nature*, vol. 207, 7 1965.

[5] M. I. Large, A. E. Vaughan, and B. Y. Mills, "A Pulsar Supernova Association?," , vol. 220, pp. 340–341, Oct. 1968.

[6] E. C. Staelin, D. H.; Reifenstein, "Pulsating radio sources near the crab nebula," *Science*, vol. 162, 12 1968.

[7] S. E. Woosley, A. Heger, and T. A. Weaver, "The evolution and explosion of massive stars," *Rev. Mod. Phys.*, vol. 74, pp. 1015–1071, 2002.

[8] R. Kippenhahn, A. Weigert, and A. Weiss, *Stellar Structure and Evolution*. Astronomy and Astrophysics Library, Springer-Verlag Berlin Heidelberg, 2nd ed., 2012.

[9] S. L. Shapiro and S. A. Teukolsky, *Black holes, white dwarfs, and neutron stars: the physics of compact objects*. Wiley, 1st ed., 1983.

[10] L. Rezzolla, P. Pizzochero, D. I. Jones, N. Rea, and I. Vidaña, *The Physics and Astrophysics of Neutron Stars*. Astrophysics and Space Science Library 457, Springer International Publishing, 1st ed., 2018.

[11] B. K. Harrison, K. S. Thorne, M. Wakano, and J. A. Wheeler, *Gravitation Theory and Gravitational Collapse*. 1965.

[12] G. M. Oppenheimer, J. R.; Volkoff, "On massive neutron cores," *Physical Review (Series I)*, vol. 55, 2 1939.

[13] R. C. Tolman, "Static Solutions of Einstein's Field Equations for Spheres of Fluid," *Physical Review*, vol. 55, pp. 364–373, Feb. 1939.

[14] A. G. Cameron, "Neutron Star Models.," , vol. 130, p. 884, Nov. 1959.

[15] N. K. G. (auth.), *Compact Stars: Nuclear Physics, Particle Physics and General Relativity*. Astronomy and Astrophysics Library, Springer US, 1996.

[16] F. Özel and P. Freire, "Masses, Radii, and the Equation of State of Neutron Stars," *Annual Review of Astronomy and Astrophysics*, vol. 54, pp. 401–440, 07 2016.

[17] LIGO Scientific Collaboration and Virgo Scientific Collaboration, "Gw170817: Observation of gravitational waves from a binary neutron star inspiral," *Physical Review Letters*, vol. 119, 10 2017.

[18] L. Rezzolla, E. R. Most, and L. R. Weih, "Using gravitational-wave observations and quasi-universal relations to constrain the maximum mass of neutron stars," *Astrophys. J.*, vol. 852, no. 2, p. L25, 2018. [Astrophys. J. Lett.852,L25(2018)].

[19] I. Arcavi *et al.*, "Energetic eruptions leading to a peculiar hydrogen-rich explosion of a massive star," 2017.

[20] D. A. Coulter *et al.*, "Swope Supernova Survey 2017a (SSS17a), the Optical Counterpart to a Gravitational Wave Source," *Science*, 2017. [Science358,1556(2017)].

[21] N. R. Tanvir *et al.*, "The Emergence of a Lanthanide-Rich Kilonova Following the Merger of Two Neutron Stars," *Astrophys. J.*, vol. 848, no. 2, p. L27, 2017.

[22] B. D. Margalit, Ben; Metzger, "Constraining the maximum mass of neutron stars from multi-messenger observations of gw170817," *The Astrophysical Journal*, vol. 850, 11 2017.

[23] B. Li, Li-Xin; Paczyński, "Transient events from neutron star mergers," *The Astrophysical Journal*, vol. 507, 11 1998.

[24] B. D. Metzger *et al.*, "Electromagnetic Counterparts of Compact Object Mergers Powered by the Radioactive Decay of R-process Nuclei," *Mon. Not. Roy. Astron. Soc.*, vol. 406, p. 2650, 2010.

[25] K. D. Alexander *et al.*, "The Electromagnetic Counterpart of the Binary Neutron Star Merger LIGO/VIRGO GW170817. VI. Radio Constraints on a Relativistic Jet and Predictions for Late-Time Emission from the Kilonova Ejecta," *Astrophys. J.*, vol. 848, no. 2, p. L21, 2017.

[26] D. Barnes, Jennifer; Kasen, "Effect of a high opacity on the light curves of radioactively powered transients from compact object mergers," *The Astrophysical Journal*, vol. 775, 09 2013.

[27] M. Tanaka and K. Hotokezaka, "Radiative Transfer Simulations of Neutron Star Merger Ejecta," *Astrophys. J.*, vol. 775, p. 113, 2013.

[28] R. Margutti *et al.*, "The Electromagnetic Counterpart of the Binary Neutron Star Merger LIGO/VIRGO GW170817. V. Rising X-ray Emission from an Off-Axis Jet," *Astrophys. J.*, vol. 848, no. 2, p. L20, 2017.

[29] T. Damour and A. Nagar, "Effective One Body description of tidal effects in inspiralling compact binaries," *Phys. Rev.*, vol. D81, p. 084016, 2010.

[30] A. Bauswein and H. T. Janka, "Measuring neutron-star properties via gravitational waves from binary mergers," *Phys. Rev. Lett.*, vol. 108, p. 011101, 2012.

[31] J. Alsing, H. O. Silva, and E. Berti, "Evidence for a maximum mass cut-off in the neutron star mass distribution and constraints on the equation of state," *Mon. Not. Roy. Astron. Soc.*, vol. 478, no. 1, pp. 1377–1391, 2018.

[32] P. D. Lasky, B. Haskell, V. Ravi, E. J. Howell, and D. M. Coward, "Nuclear Equation of State from Observations of Short Gamma-Ray Burst Remnants," *Phys. Rev.*, vol. D89, no. 4, p. 047302, 2014.

[33] B. D. Fernández, Rodrigo; Metzger, "Electromagnetic signatures of neutron star mergers in the advanced ligo era," *Annual Review of Nuclear and Particle Science*, vol. 66, 11 2016.

[34] A. Bauswein, T. W. Baumgarte, and H. T. Janka, "Prompt merger collapse and the maximum mass of neutron stars," *Phys. Rev. Lett.*, vol. 111, no. 13, p. 131101, 2013.

[35] M. Ruffert, H. T. Janka, K. Takahashi, and G. Schaefer, "Coalescing neutron stars: A Step towards physical models. 2. Neutrino emission, neutron tori, and gamma-ray bursts," *Astron. Astrophys.*, vol. 319, pp. 122–153, 1997.

[36] S. Wanajo, Y. Sekiguchi, N. Nishimura, K. Kiuchi, K. Kyutoku, and M. Shibata, "Production of all the r-process nuclides in the dynamical ejecta of neutron star mergers," *Astrophys. J.*, vol. 789, p. L39, 2014.

[37] A. Perego, S. Rosswog, R. M. Cabezón, O. Korobkin, R. Käppeli, A. Arcones, and M. Liebendörfer, "Neutrino-driven winds from neutron star merger remnants," *Mon. Not. Roy. Astron. Soc.*, vol. 443, no. 4, pp. 3134–3156, 2014.

[38] M. Nicholl *et al.*, "The Electromagnetic Counterpart of the Binary Neutron Star Merger LIGO/VIRGO GW170817. III. Optical and UV Spectra of a Blue Kilonova From Fast Polar Ejecta," *Astrophys. J.*, vol. 848, no. 2, p. L18, 2017.

[39] R. Chornock *et al.*, "The Electromagnetic Counterpart of the Binary Neutron Star Merger LIGO/VIRGO GW170817. IV. Detection of Near-infrared Signatures of r-process Nucleosynthesis with Gemini-South," *Astrophys. J.*, vol. 848, no. 2, p. L19, 2017.

[40] P. S. Cowperthwaite *et al.*, "An Empirical Study of Contamination in Deep, Rapid, and Wide-Field Optical Follow-Up of Gravitational Wave Events," *Astrophys. J.*, vol. 858, no. 1, p. 18, 2018.

[41] R. Fernández, F. Foucart, D. Kasen, J. Lippuner, D. Desai, and L. F. Roberts, "Dynamics, nucleosynthesis, and kilonova signature of black hole—neutron star merger ejecta," *Class. Quant. Grav.*, vol. 34, no. 15, p. 154001, 2017.

[42] A. I. MacFadyen, S. E. Woosley, and A. Heger, "Supernovae, jets, and collapsars," *Astrophys. J.*, vol. 550, p. 410, 2001.

[43] D. Eichler, M. Livio, T. Piran, and D. N. Schramm, "Nucleosynthesis, Neutrino Bursts and Gamma-Rays from Coalescing Neutron Stars," *Nature*, vol. 340, pp. 126–128, 1989. [,682(1989)].

[44] A. Goldstein *et al.*, "An Ordinary Short Gamma-Ray Burst with Extraordinary Implications: Fermi-GBM Detection of GRB 170817A," *Astrophys. J.*, vol. 848, no. 2, p. L14, 2017.

[45] W. Fong *et al.*, "The Electromagnetic Counterpart of the Binary Neutron Star Merger LIGO/VIRGO GW170817. VIII. A Comparison to Cosmological Short-duration Gamma-ray Bursts," *Astrophys. J.*, vol. 848, no. 2, p. L23, 2017.

[46] E. Berger, "Short-duration gamma-ray bursts," *Annual Review of Astronomy and Astrophysics*, vol. 52, 08 2014.

[47] A. Murguia-Berthier, G. Montes, E. Ramirez-Ruiz, F. De Colle, and W. H. Lee, "Necessary Conditions for Short Gamma-Ray Burst Production in Binary Neutron Star Mergers," *Astrophys. J.*, vol. 788, p. L8, 2014.

[48] M. Shibata, "Constraining nuclear equations of state using gravitational waves from hypermassive neutron stars," *Phys. Rev. Lett.*, vol. 94, p. 201101, 2005.

[49] K. Hotokezaka, K. Kyutoku, H. Okawa, M. Shibata, and K. Kiuchi, "Binary Neutron Star Mergers: Dependence on the Nuclear Equation of State," *Phys. Rev.*, vol. D83, p. 124008, 2011.

[50] T. W. Baumgarte, S. L. Shapiro, and M. Shibata, "On the maximum mass of differentially rotating neutron stars," *Astrophys. J.*, vol. 528, p. L29, 2000.

[51] V. Paschalidis, Z. B. Etienne, and S. L. Shapiro, "Importance of cooling in triggering the collapse of hypermassive neutron stars," *Phys. Rev.*, vol. D86, p. 064032, 2012.

[52] J. D. Kaplan, C. D. Ott, E. P. O'Connor, K. Kiuchi, L. Roberts, and M. Duez, "The influence of thermal pressure on equilibrium models of hypermassive neutron star merger remnants," *The Astrophysical Journal*, vol. 790, 07 2014.

[53] N. Bucciantini, B. D. Metzger, T. A. Thompson, and E. Quataert, "Short GRBs with Extended Emission from Magnetar Birth: Jet Formation and Collimation," *Mon. Not. Roy. Astron. Soc.*, vol. 419, p. 1537, 2012.

[54] B. Giacomazzo and R. Perna, "Formation of Stable Magnetars from Binary Neutron Star Mergers," *Astrophys. J.*, vol. 771, p. L26, 2013.

[55] M. Ruffert and H. T. Janka, "Gamma-ray bursts from accreting black holes in neutron star mergers," *Astron. Astrophys.*, vol. 344, pp. 573–606, 1999.

[56] M. Shibata and K. Taniguchi, "Merger of binary neutron stars to a black hole: disk mass, short gamma-ray bursts, and quasinormal mode ringing," *Phys. Rev.*, vol. D73, p. 064027, 2006.

[57] R. Fernández and B. D. Metzger, "Delayed outflows from black hole accretion tori following neutron star binary coalescence," *Mon. Not. Roy. Astron. Soc.*, vol. 435, p. 502, 2013.

[58] Y. Sekiguchi, K. Kiuchi, K. Kyutoku, M. Shibata, and K. Taniguchi, "Dynamical mass ejection from the merger of asymmetric binary neutron stars: Radiation-hydrodynamics study in general relativity," *Phys. Rev.*, vol. D93, no. 12, p. 124046, 2016.

[59] K. Kiuchi, K. Kyutoku, Y. Sekiguchi, M. Shibata, and T. Wada, "High resolution numerical-relativity simulations for the merger of binary magnetized neutron stars," *Phys. Rev.*, vol. D90, p. 041502, 2014.

[60] L. Stella, S. Dall'Osso, G. Israel, and A. Vecchio, "Gravitational radiation from newborn magnetars," *Astrophys. J.*, vol. 634, pp. L165–L168, 2005.

[61] S. Dall'Osso, S. N. Shore, and L. Stella, "Early evolution of newly born magnetars with a strong toroidal field," *Mon. Not. Roy. Astron. Soc.*, vol. 398, p. 1869, 2009.

[62] J. Braithwaite, "Axisymmetric magnetic fields in stars: relative strengths of poloidal and toroidal components," *Mon. Not. Roy. Astron. Soc.*, vol. 397, p. 763, 2009.

[63] N. Yagi, K.; Yunes, "I-love-q: Unexpected universal relations for neutron stars and quark stars," *Science*, vol. 341, 07 2013.

[64] C. Breu and L. Rezzolla, "Maximum mass, moment of inertia and compactness of relativistic stars," *Mon. Not. Roy. Astron. Soc.*, vol. 459, no. 1, pp. 646–656, 2016.

[65] K. Yagi and N. Yunes, "Approximate Universal Relations for Neutron Stars and Quark Stars," *Phys. Rept.*, vol. 681, pp. 1–72, 2017.

[66] F. X. Timmes, S. E. Woosley, and T. A. Weaver, "The Neutron star and black hole initial mass function," *Astrophys. J.*, vol. 457, p. 834, 1996.

[67] M. Hanauske, K. Takami, L. Bovard, L. Rezzolla, J. A. Font, F. Galeazzi, and H. Stöcker, "Rotational properties of hypermassive neutron stars from binary mergers," *Phys. Rev.*, vol. D96, no. 4, p. 043004, 2017.

[68] M. Shibata, S. Fujibayashi, K. Hotokezaka, K. Kiuchi, K. Kyutoku, Y. Sekiguchi, and M. Tanaka, "Modeling GW170817 based on numerical relativity and its implications," *Phys. Rev.*, vol. D96, no. 12, p. 123012, 2017.

[69] J. Antoniadis *et al.*, "A Massive Pulsar in a Compact Relativistic Binary," *Science*, vol. 340, p. 6131, 2013.

[70] N. Stergioulas and J. Friedman, "Comparing models of rapidly rotating relativistic stars constructed by two numerical methods," *Astrophys. J.*, vol. 444, p. 306, 1995.

[71] A. Bauswein, O. Just, H.-T. Janka, and N. Stergioulas, "Neutron-star radius constraints from GW170817 and future detections," *Astrophys. J.*, vol. 850, no. 2, p. L34, 2017.

[72] A. Bauswein and N. Stergioulas, "Semi-analytic derivation of the threshold mass for prompt collapse in binary neutron star mergers," *Mon. Not. Roy. Astron. Soc.*, vol. 471, no. 4, pp. 4956–4965, 2017.

[73] M. Ruiz, S. L. Shapiro, and A. Tsokaros, "GW170817, General Relativistic Magnetohydrodynamic Simulations, and the Neutron Star Maximum Mass," *Phys. Rev.*, vol. D97, no. 2, p. 021501, 2018.

[74] J. D. Kaplan, C. D. Ott, E. P. O'Connor, K. Kiuchi, L. Roberts, and M. Duez, "The Influence of Thermal Pressure on Equilibrium Models of Hypermassive Neutron Star Merger Remnants," *Astrophys. J.*, vol. 790, p. 19, 2014.

[75] H. T. Cromartie *et al.*, "Relativistic Shapiro delay measurements of an extremely massive millisecond pulsar," 2019.